# EVALUATION OF AEROMAGNETIC ANOMALIES OF BASHAR AND ITS ENVIRONS, NORTHCENTRAL NIGERIA

Supported by tetfund TERTIARY EDUCATION TRUST FUND

**Zumji Julius Jilang[1]*, Odewumi, Shola Christopher[2] and Akanbi, Eti-mbuk Stella[1]**
[1]Department of Physics, University of Jos, Nigeria
[2]Department of Science Laboratory Technology, University of Jos, Nigeria
*Corresponding author: zumji4u@gmail.com

**Received:** September 08, 2021 **Accepted:** November 01, 2021

Abstract: The Quantitative Interpretations of Aeromagnetic Data of Bashar and its environs, northcentral Nigeria were carried out with the aim of determining the Curie Point Depth, Geothermal Gradient, Heat Flow, and depth to magnetic source. The geomagnetic gradient was removed from the aeromagnetic data using the International Geomagnetic Reference Field (IGRF) and the obtained data were shown as Total Magnetic Intensity (TMI) maps. Software used for the analysis include: Oasis Montaj Version 8.4, Matlab Version R2010a, Grapher 5, SUFER 11, Georient and Microsoft Excel. The Total Magnetic Intensity (TMI) map has an intensity ranges from 32876.4 to 33189.7 nT, showing significant magnetic high and low signatures. The Reduce-to-Equator (RTE) map has an intensity range of -732.6 to -405.5 nT. The heat flow increases with decrease in Curie point depth, and the Curie depths vary from 5.19 to 9.53 km. The heat flow values are suggestive of anomalous geothermal conditions and are recommended for detailed geothermal exploration. However, the geothermal gradient varies from 60.86 to 111.75$^{o}$C km$^{-1}$ and heat flow value ranges from 152.15 to 279.38 mWm$^{-2}$. The average geothermal gradients and heat flow is an indication that the area is suitable for harnessing of geothermal energy, which could be used to generate electricity.

**Keywords:** Heat flow, geothermal, curie, energy and electricity

## Introduction

Aeromagnetic survey is a procedure that involves carrying out a comparative rapid and large-scale magnetic survey using a magnetometer affix to an aircraft. The aircraft typically flies in a grid-like pattern which measures and records the total intensity of the magnetic field at the sensor, with height and line spacing determining the resolution of the data. According to Reeve (2005), this measurement is a combination of the earth's core field (documented worldwide as the International Geomagnetic Reference Field, IGRF) and the field induced in crustal rocks. It maps out the variations in geomagnetic field, which occurs due to the changes in the percentage of magnetite in rock.

The variations in the measured magnetic field reflect the distribution of magnetic minerals (mainly magnetite) in the Earth's crust. Human-made objects and surveys can be used to detect, locate and characterize these magnetic sources. Aeromagnetic surveys are largely applied in subsurface exploration, environmental and ground-water investigation, and geological mapping. This study focuses on Quantitative Interpretations of Aeromagnetic Data of Bashar and its environs, northcentral Nigeria with the aim of determining the Curie Point Depth, Geothermal Gradient, Heat Flow, and depth to magnetic source.

## Location and geological setting of the study area

The study area is located on Latitudes $9^{0}00^{l}$ to $9^{0}30^{l}$ N, and Longitudes $9^{0}30^{l}$ to $10^{0}30^{l}$ E with an approximate area of 6,050 km$^{2}$. The study area comprises of the Precambrian Basement rocks, Younger Granite Ring complexes and part of the middle Benue Trough in northcentral Nigeria. The study area has two distinctive relief features: lowlands and highlands as shown in the Digital Elevation Map of the study area (Fig. 1). Generally, the area is characterized by a rugged relief (hills and undulating plains).

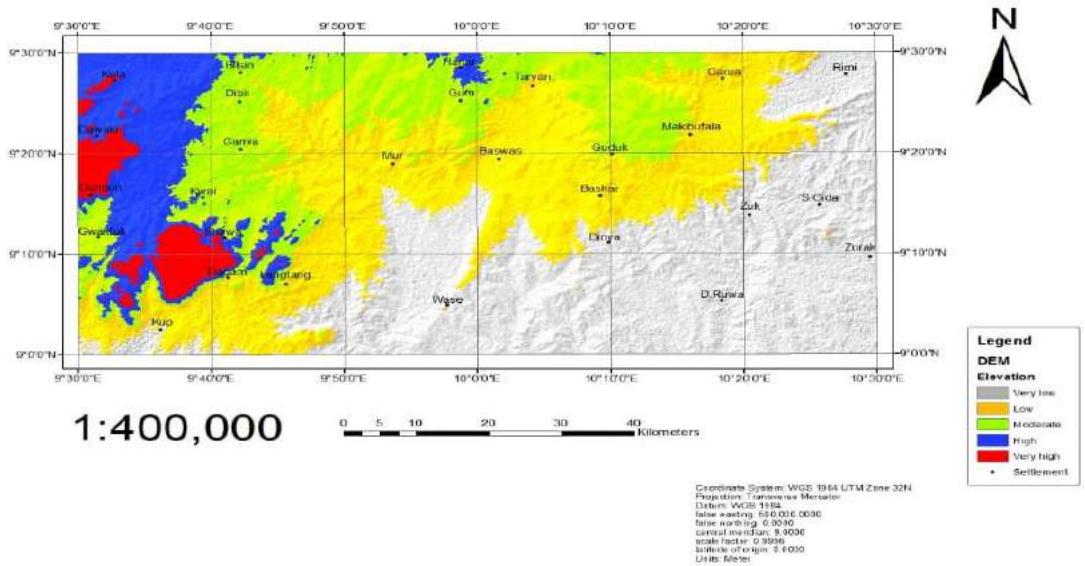


**Fig. 1: Digitized Elevation Map of the study area (Extracted from Topography Map Published by Federal Surveys of Nigeria, 1962)**

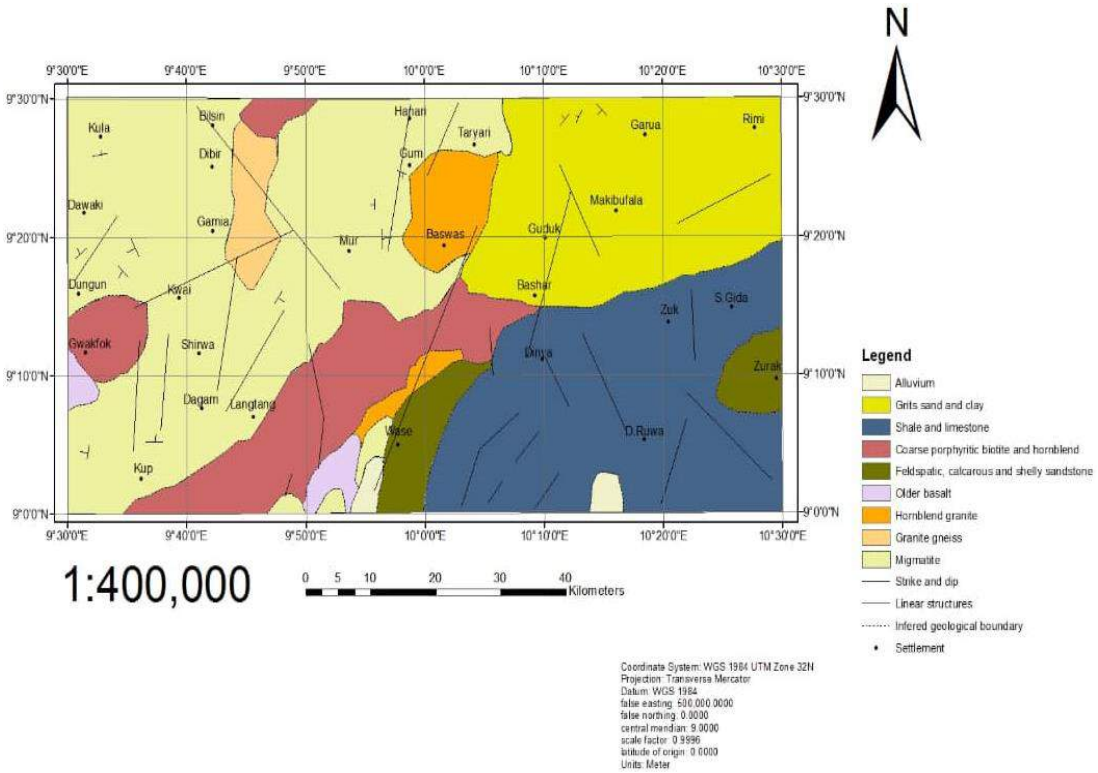


**Fig. 2: Geological Map of Wase Sheet 191 and Bashar Sheet 192**

The geology map of the study area is shown in Fig. 2. The Precambrian Basement Complex is unconformably overlain by the BimaBandstone which is the oldest and the most extensively outcropping formation in the Benue trough (Carter *et al*., 1963) According to Oyawoye (1964), the area consists of gneiss migmatites, and the Older Granite. Jacobson *et al*. (1963) also reported that the rock found within the study area comprises of migmatites, granite-gniesses and Older granite. This group of rock is believed to be as a result of remobilization during the Pan-African Orogeny. The Younger Granite occurs largely as distinct pluton often batholitic size ranging in composition from quartz-hypersthenes diorite through leucocratic granites, porphyriticbiotite Granite, granodiorite and pegmatite.

In the eastern part of the study area, the Precambrian to lower Paleozoic basement gneisses and migmatite were overlain by alternating shale, limestone, shelly sandstones and clay. The sandstones consist of slightly cemented fine coarse grained sandstone and clay with interbeded thin beds of carbonaceous shale and clays.

**Materials and Methods**

The software used include the following: Oasis Montaj version 8.4 (2015); MatLap (2015); Grapher 5 (2004); ILWIS 3.3 (2005); Surfer 11 (2011) and Microsoft Excel (2016). Interpretation of the aeromagnetic survey data aims to map the surface and subsurface regional structures (e.g., faults, contacts, bodies and mineralization). Aeromagnetic data are mostly analyzed in these processes: Aeromagnetic data filtration (upward and/ or downward continuation, Reduction to pole, Reduction to equator, vertical derivatives, etc.), Regional-Residual Separation, and Depth estimation analysis

The Standard 3D Euler method is based on Euler's homogeneity equation, which relates the potential Field (magnetic or gravity) and its gradient components to the location of the sources, by the degree of homogeneity N, which can be interpreted as a structural index (Thompson, 1982). The method makes use of a structural index in addition to producing depth estimates. The objective of the Euler deconvolution process is to produce a map showing the locations and the corresponding depth estimations of geologic sources of magnetic or gravimetric anomalies in a two-dimensional grid (Reid *et al*., 1990). In combination, the structural index and the depth estimates have the potential to identify and calculate depth estimates for a variety of geologic structures such as faults, magnetic contacts, dykes, sills, etc. The algorithm uses a least squares method to solve Euler's equation simultaneously for each grid position within a sub-grid.

A square window of predefined dimensions (number of grid cells) is moved over the grid along each row. At each grid point a system of equations are solved, from which the four unknowns (x, y as location in the grid, z as depth estimation and the background value) and their uncertainties (standard deviation) are obtained for a given structural index. A solution is only recorded if the depth uncertainty of the calculated depth estimate is less than a specified threshold and the location of the solution is within a limiting distance from the center of the data window. Thompson (1982) showed that for any homogenous, three-dimensional function f (x; y; z) of degree n:

$$f(tx, ty, tz) = t^n f(x, y, z) \quad (1)$$

In general, for a homogenous function of *x*, *y*, *z*... of degree *n*, it is always the case that:

$$x\frac{\delta f}{\delta x} + y\frac{\delta f}{\delta y} + z\frac{\delta f}{\delta z} = nf \quad (2)$$

In geophysics, the function $f$(x, y, z) can have the general functional form:

$$f(x, y, z) = \frac{G}{r^N} \quad (3)$$

**Where**

$$r^2 = (x - x_o)^2 + (y - y_o)^2 + (z - z_o)^2, \quad (4)$$

N is a real number (1, 2, 3...) and G is a constant (independent of x, y, z). Many simple point magnetic sources can be described by equation (3),

**Where** ($x_o$; $y_o$; $z_o$) is the position of the source whose field F is measured.

The method of using spectral analysis in depth determination is based on the principle that a magnetic field measured at the surface can be considered the integral of magnetic signatures from all depths. The power spectrum computes the thickness of the sedimentary basin and that of the crustal Moho depth (Spector and Grant, 1970). Given a residual magnetic anomaly map of dimension L x L digitized at equal intervals, the residual intervals, and total intensity anomaly values can be expressed in terms of double Fourier series expansion, which is given by:

$$T(x,y) = \sum_{n=1}^{N}\sum_{m=1}^{M} P_m^n \left[\cos\left(\frac{2\pi}{l}\right)(nx+my)\right] + Q_m^n \sin\left[\left(\frac{2\pi}{l}\right)(nx+my)\right] \quad (5)$$

**Where:** lis the dimension of the block, $P_m^n and Q_m^n$ are the Fourier amplitudes while N, M represent the number of grid points along the x and y directions respectively. Equation (5) can be combined into a single partial wave thus:

$$\cos\left[\left(\frac{2\pi}{l}\right)(nx+my)\right] + Q_m^n \sin\left[\left(\frac{2\pi}{l}\right)(nx+my)\right] = C_m^n \cos\left[\left(\frac{2\pi}{l}\right)(nx+my) - \delta_m^n\right] \quad (6)$$

**Where** $(P_m^n)^2 + (Q_m^n)^2 = (C_m^n)^2 and \delta_m^n$ is the appropriate phase angle. Each ($C_m^n$) is amplitude of the partial wave. The frequency of this wave is given by

$$F_m^n = \sqrt{n^2 + m^2}$$

The filtered Reduced to Equator (RTE) as shown in Fig. 5 from the crustal field map was divided into eight square grids and each window grid was 27.5 x 27.5 km in size (Fig. 6). The estimation of the Curie point depth was based on spectral analysis of the reduced to equator data. To minimize the effect of frequency noise caused by tiny structures near ground surface, the RTE anomaly map was upward continued to 15 km to determine the regional field at curie point isotherm. Bhattacharyya and Leu (1975) presented that depth to bottom ($z_b$) of a magnetic source body could be estimated using two methods. Firstly, by estimation of depth to the centroid ($z_0$) and secondly, estimation of depth to the top ($Z_t$) of the magnetic sources which was quantitatively computed.

The lower bound ($Z_b$) of the magnetic source corresponding to Curie point depth was derived from the equation given by Bhattacharyya and Leu (1975) as:

$$Z_b = 2Z_o - Z_t \quad (1)$$

The geothermal gradient (dT/dZ) between the earth and the Curie point depth ($Z_b$) was defined by the equation:

$$\frac{dT}{dZ} = \frac{580^{\circ}C}{Z_b} \quad (2)$$

**Where** 580°C is the Curie temperature at which ferromagnetic minerals are converted to paramagnetic minerals. The geothermal gradient was related to heat flow (q) using the formula: Where λ is the coefficient of thermal conductivity.

$$q = \lambda\left(\frac{dT}{dZ}\right) = \lambda\left(\frac{580^{\circ}C}{Z_b}\right) \quad (3)$$

A thermal conductivity of 2.5 $mWm^{-2}$ given by Stacy (1977) as the average value for igneous rocks was used to compute the subsurface heat flow. The data so obtained from the computations was used to generate the Curie isotherm depth, heat flow and geothermal gradient map.

**Results and Discussion**

The total magnetic intensity (TMI) value ranges from 32876.4 to 33189.7 nT (Fig. 3) and Residual aeromagnetic intensity map (Fig. 4) of Bashar area revealed variations in magnetic field intensity throughout the area with values of the residual map ranges from -732.6 to -405.4 nT. The magnetic intensity of RTE map ranges from -732.6 to - 405.5 nT as shown in Fig. 5.

To determine the depths of the anomalous magnetic sources, the RTE map of the study area was divided into 32 overlapping grids (Fig. 6). The locations of these grids and the computed spectral depths are presented in Table 1 with $X_1$ and $X_2$ as the limiting longitudes while $Y_1$ and $Y_2$ indicating the limiting latitudes for each of the blocks. Each of these spectral blocks covers a square area of about 13.85 x 13.85 km of the data sheet.

**Table 1: Spectral depth estimates to magnetic basement over Wase and Bashar (D1=Deeper source and D2= Shallow source)**

| S/N | Spectral Block | Longitude | | Latitude | | Spectral Depth (km) | |
|---|---|---|---|---|---|---|---|
| | | $X_1$ | $X_2$ | $Y_1$ | $Y_2$ | $D_1$ | $D_2$ |
| 1 | 1 | 9.5 | 9.65 | 9.375 | 9.5 | 0.447 | 0.316 |
| 2 | 2 | 9.65 | 9.75 | 9.375 | 9.5 | 0.283 | 0.44 |
| 3 | 3 | 9.75 | 9.875 | 9.375 | 9.5 | 0.961 | 0.247 |
| 4 | 4 | 9.875 | 10.0 | 9.375 | 9.5 | 0.961 | 0.307 |
| 5 | 5 | 10.0 | 10.125 | 9.375 | 9.5 | 1.6 | 0.357 |
| 6 | 6 | 10.125 | 10.25 | 9.375 | 9.5 | 2.25 | 0.324 |
| 7 | 7 | 10.25 | 10.375 | 9.375 | 9.5 | 0.69 | 0.326 |
| 8 | 8 | 10.375 | 9.5 | 9.375 | 9.5 | 2.16 | 0.547 |
| 9 | 9 | 9.5 | 9.625 | 9.25 | 9.375 | 1.18 | 0.354 |
| 10 | 10 | 9.625 | 9.75 | 9.25 | 9.375 | 0.659 | 0.268 |
| 11 | 11 | 9.75 | 9.875 | 9.25 | 9.375 | 2.05 | 0.319 |
| 12 | 12 | 9.875 | 10.0 | 9.25 | 9.375 | 1.11 | 0.263 |
| 13 | 13 | 10.0 | 10.125 | 9.25 | 9.375 | 0.757 | 0.28 |
| 14 | 14 | 10.125 | 10.25 | 9.25 | 9.375 | 0.79 | 0.282 |
| 15 | 15 | 10.25 | 10.375 | 9.25 | 9.375 | 1.36 | 0.33 |
| 16 | 16 | 10.375 | 9.5 | 9.25 | 9.375 | 1.53 | 0.295 |
| 17 | 17 | 9.5 | 9.625 | 9.125 | 9.25 | 1.51 | 0.295 |
| 18 | 18 | 9.625 | 9.75 | 9.125 | 9.25 | 1.33 | 0.461 |
| 19 | 19 | 9.75 | 9.875 | 9.125 | 9.25 | 2.40 | 0.403 |
| 20 | 20 | 9.875 | 10.0 | 9.125 | 9.25 | 1.06 | 0.325 |
| 21 | 21 | 10.0 | 10.125 | 9.125 | 9.25 | 1.24 | 0.297 |
| 22 | 22 | 10.125 | 10.25 | 9.125 | 9.25 | 0.708 | 0.202 |
| 23 | 23 | 10.25 | 10.375 | 9.125 | 9.25 | 1.64 | 0.291 |
| 24 | 24 | 10.375 | 9.5 | 9.125 | 9.25 | 0.939 | 0.305 |
| 25 | 25 | 9.5 | 9.625 | 9.0 | 9.125 | 0.914 | 0.323 |
| 26 | 26 | 9.625 | 9.75 | 9.0 | 9.125 | 1.24 | 0.337 |
| 27 | 27 | 9.75 | 9.875 | 9.0 | 9.125 | 0.896 | 0.282 |
| 28 | 28 | 9.875 | 10.0 | 9.0 | 9.125 | 0.556 | 0.199 |
| 29 | 29 | 10.0 | 10.125 | 9.0 | 9.125 | 3.04 | 0.283 |
| 30 | 30 | 10.125 | 10.25 | 9.0 | 9.125 | 2.35 | 0.344 |
| 31 | 31 | 10.25 | 10.375 | 9.0 | 9.125 | 2.41 | 0.290 |
| 32 | 32 | 10.375 | 10.5 | 9.0 | 9.125 | 2.78 | 0.581 |
| **Average** | | | | | | **1.367** | **0.327** |

The representative plots of the power spectrum of Wase and Bashar Sheets are represented as graphs of logarithms of spectral energies against frequency. Each of these plots revealed a two-layer depth model as represented by two clear segments. Thus, the logarithmic plot of a radial spectrum would give a straight line whose slope is 2z. From the gradients of the segments the average depths to the causative layers were determined as $D_1$ and $D_2$ (Table 1).

The first layer depth $D_1$ (deeper depth), represents the depth to the magnetic basement (sedimentary thickness) while $D_2$ (shallow depth) is the shallow magnetic sources represented by the second line segment of the power spectrum plots. The depth to the first layer ($D_1$) varies from 0.283 to 3.04 km (Fig. 7) with an average depth of 1.367 km (Table 1) and this layer

may be attributed to magnetic rocks of the basement, lateral variations in basement susceptibilities and intra- basement features like faults and fractures. The deeper magnetic depth source ($D_1$) suggests the occurrence of Precambrian Basement rocks and was confirmed with TMI values which indicate Migmatite-Gneiss Complex.

The second layer depth ($D_2$) which represents the shallow depth varies from 0.202 to 0.547 km with the average depth of 0.327 km (Fig. 8) and could be attributed to near surface magnetic sources, which are magnetic rocks that intruded into the sedimentary formations. Shallow magnetic sources could either be as a result of near surface intrusive and can be closely related to the tectonic and structural evolution of the study area or basement rocks that were tectonically uplifted into the sedimentary overburden. The deeper basement depths may be attributed to lateral inversions in basement susceptibilities and intra basement structural deformations like faults and fractures (Ofoegbu and Onuoha, 1991; Kangoko *et al*., 1997).

The crustal map was also divided into eight (8) overlapping square blocks (Fig. 4). Each square block was subjected to power spectral plots of energies versus frequencies using Oasis Montaj version 8.4. From the graphs of the Logarithm of spectral energies versus frequencies plotted for each of the eight blocks shows there were spectral peaks which were easily noticeable and the significance of this is the indication of the fact that Curie point depths are detectable as it defines the source bottoms.

The depth to the Centroid ($Z_0$) ranges from 12.12 to 15.29 km as presented in Table 2. On the other hand, the depth to the top boundary (Zt) of magnetic sources ranges from 0.3569 to 3.26 km and the equivalent curie depth ($Z_b$) ranges from 6.653 to 6.540 km. The average curie depth is 7.28 km and shallowest curie depth of 5.19 km was observed in block 5 when compared to the other part of the study area. The shallow Curie depth observed could be as a result of the intruded Older Granite unit identified in the area.

From the relation of $Z_b=2Z_0$-Zt, the CPD ($Z_b$) of this present work was computed for each block in other to estimates the average bottom depth of magnetic sources (Table 2) and it is believed they reflect the thermal structure of the region. Similarly, the geothermal gradient varies from $87.18C^0$/km to 88.69°C/km with an average value of 82.92°C/km (Fig. 9), while heat flow parameters varies from 217.95 to 221.71 mW/m$^2$ (Fig. 10) with an average value of 207.30 mW/m$^2$, respectively (Table 2). The geothermal gradient (*dT/dZ*) was calculated and found to be 80$^o$C km$^{-1}$, while the heat flow of the study area is 200 mWm$^{-2}$. In this calculation, the Curie point temperature was assumed to be 58$^o$C and thermal conductivity 2.5 Wm$^{-1}$°C$^{-1}$ as an average value for the igneous rocks over basement. Figure 11 shows the estimated Curie point Depth

However, results of Curie Point Depth in conjunction with heat flow values revealed a distinct inverse relationship as heat flow increases with decrease in Curie point depth, and vice-versa (Table 2). All the current literature stated that the Curie point depth and heat flows are greatly dependent upon geological conditions. Heat flow is the primary observable parameter in geothermal exploration. Generally, the units that comprise high heat flow values correspond to volcanic and metamorphic regions since these two units have high heat conductivities. Additionally, tectonically active regions affect heat flows significantly (Tanaka *et al*., 1999).

The average heat flow in thermally normal continental regions was reported to be above 60 mW m$^{-2}$ while values in excess of about 80-100 mW m$^{-2}$ indicate anomalous geothermal conditions. This indicates that anomalous high heat flow geothermal values of 217.95 to 221.71 mW/m$^2$ was observed in the study area.

Euler solution was applied to the aeromagnetic data covering the study area in determining the depth to the magnetic sources, by using different structural index 0 (Fig. 12), structural index 1 (Fig. 13), structural index 2 (Fig. 14) and structural index 3 (Fig. 15) were generated. Some of the geological models chosen were dyke, cylinder and sphere models, thus the reason behind choosing structural indices of 1, 2 and 3. The result for magnetic dykes of structural index 1 (Fig. 13) shows a sedimentary thickness (depth) values ranging from -585.2 to 1029.7 m. Similarly, structural index 2 of Euler solution indicates cylindrical geological models (Fig. 14) with depth of -757.9 to 1558.5 m. On the other hand, sedimentary thickness which falls between -920.3 and 2075.2 m were revealed with structural index 3 (Fig. 15).

**Table 2: Values of depth to top (Zt), centroid depth (Z0), Curie depth (Zb), geothermal gradient (0C km-1) and heat flow from study area**

| S/N | Spectral Block | Longitude | | Latitude | | $Z_0$ (Km) | $Z_t$ (Km) | $Z_b$ (Km) | Geothermal gradient | Heat flow (mW m$^{-2}$) |
|---|---|---|---|---|---|---|---|---|---|---|
| | | $X_1$ | $X_2$ | $Y_1$ | $Y_2$ | | | | | |
| 1 | 1A | 9.5 | 9.75 | 9.25 | 9.5 | 3.501 | 0.349 | 6.653 | 87.18 | 217.95 |
| 2 | 2A | 9.75 | 10.0 | 9.25 | 9.5 | 3.57 | 0.861 | 6.279 | 92.37 | 230.9 |
| 3 | 3A | 10.0 | 10.25 | 9.25 | 9.5 | 5.51 | 1.49 | 9.53 | 60.86 | 152.15 |
| 4 | 4A | 10.25 | 9.5 | 9.25 | 9.5 | 5.39 | 1.73 | 9.05 | 64.09 | 160.22 |
| 5 | 5A | 9.5 | 9.75 | 9.0 | 9.25 | 3.07 | 0.95 | 5.19 | 111.75 | 279.38 |
| 6 | 6A | 9.75 | 10.0 | 9.0 | 9.25 | 3.61 | 0.909 | 6.311 | 91.90 | 229.75 |
| 7 | 7A | 10.0 | 10.25 | 9.0 | 9.25 | 4.80 | 0.881 | 8.719 | 66.52 | 166.303 |
| 8 | 8A | 10.25 | 10.5 | 9.0 | 9.25 | 3.64 | 0.74 | 6.54 | 88.69 | 221.71 |
| | **Average** | | | | | **4.14** | **0.99** | **7.28** | **82.92** | **207.30** |

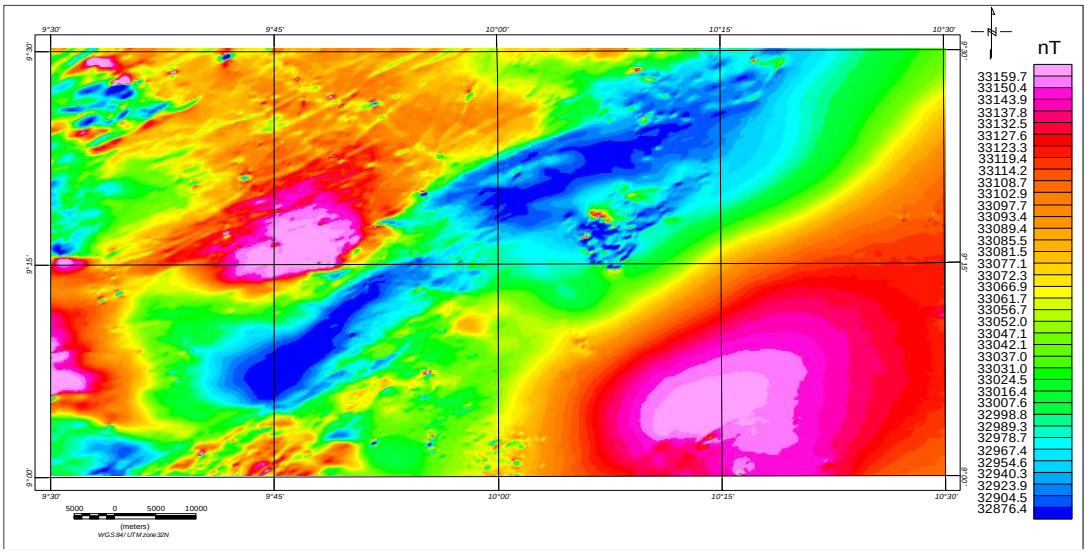


**Fig. 3: Total magnetic intensity (TMI) map of the study area**

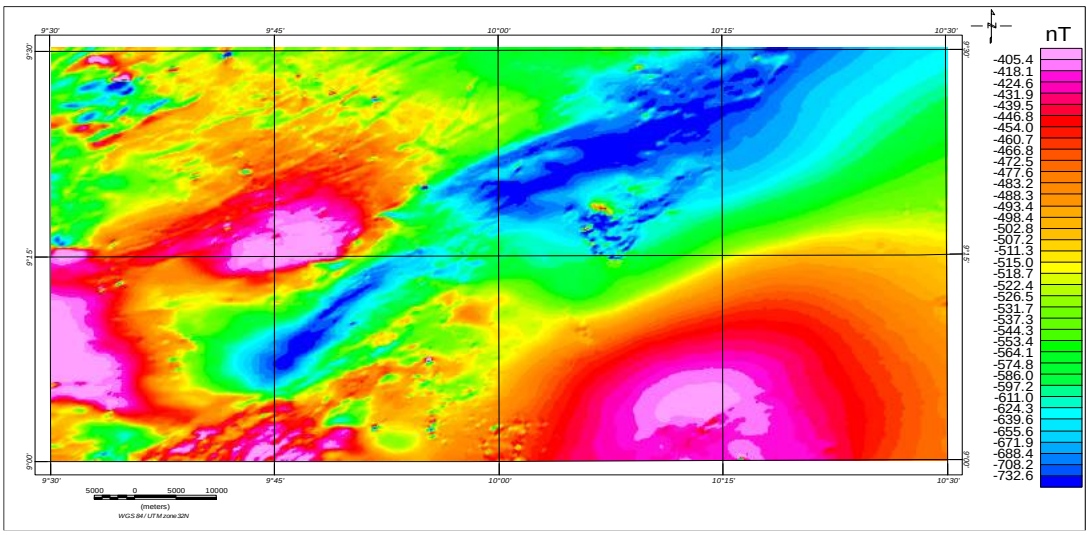


**Fig. 4: Residual map (crustal field) of the study area**

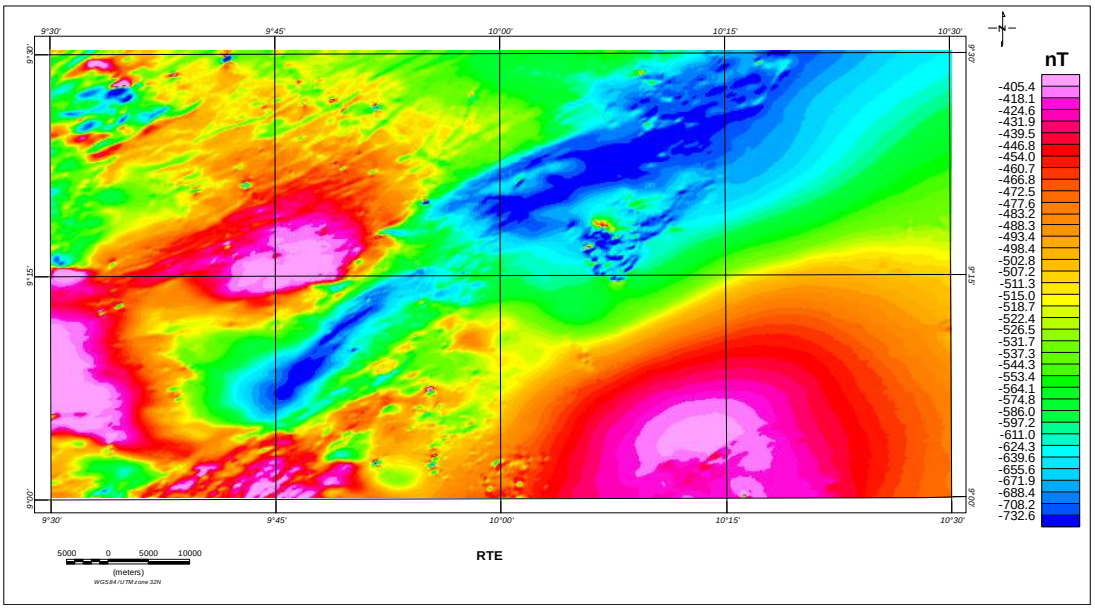


**Fig. 5: Reduced-to-equator map of the study area**

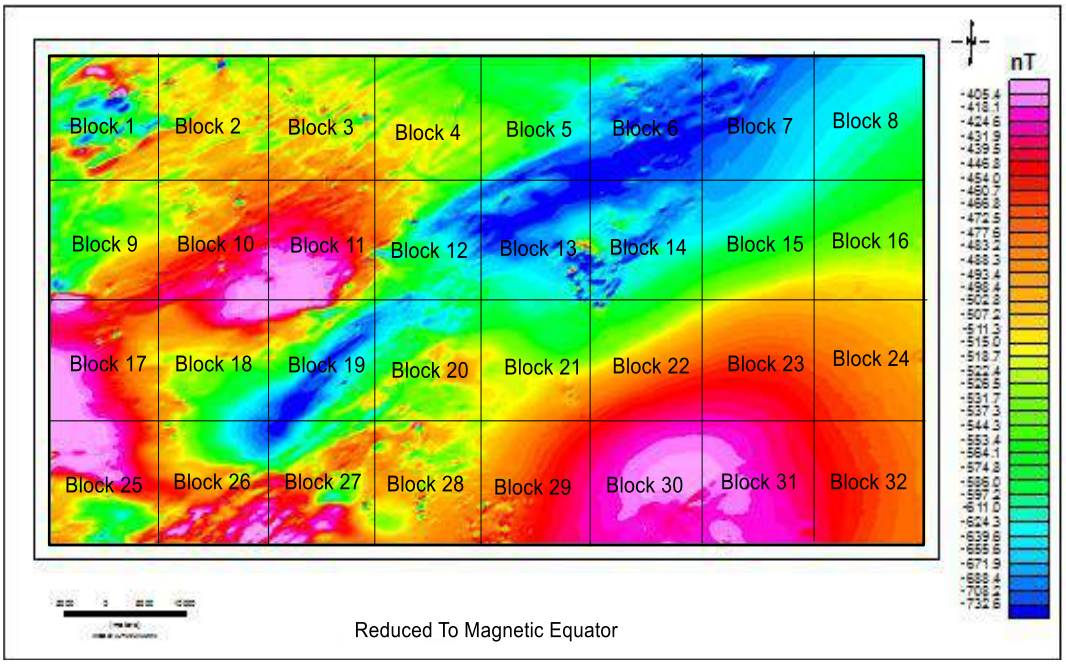


**Fig. 6: Showing 32 overlapping grids blocks of the study area**

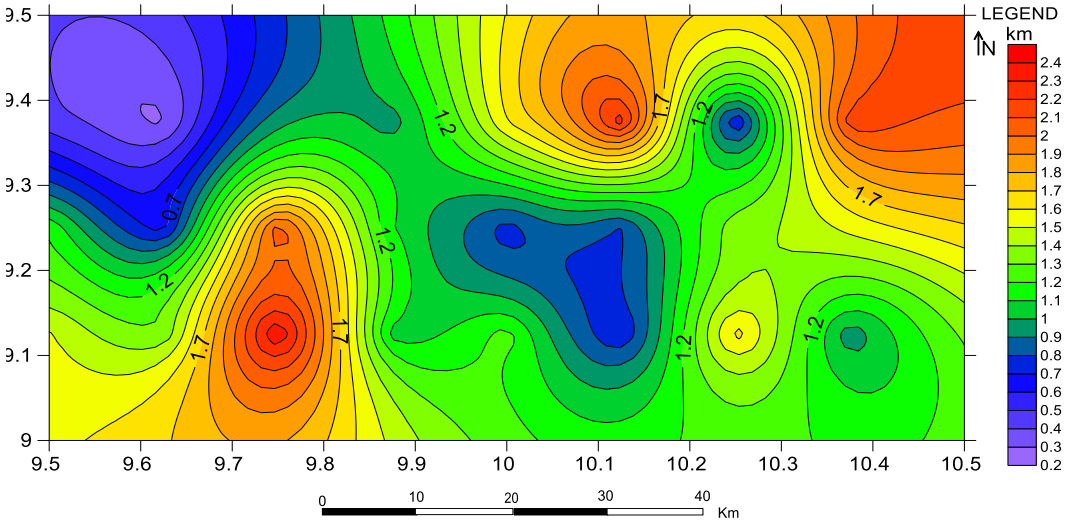


**Fig. 7: Spectral plots for all $D_1$ showing maximum depth of 2.4 km of the study area**

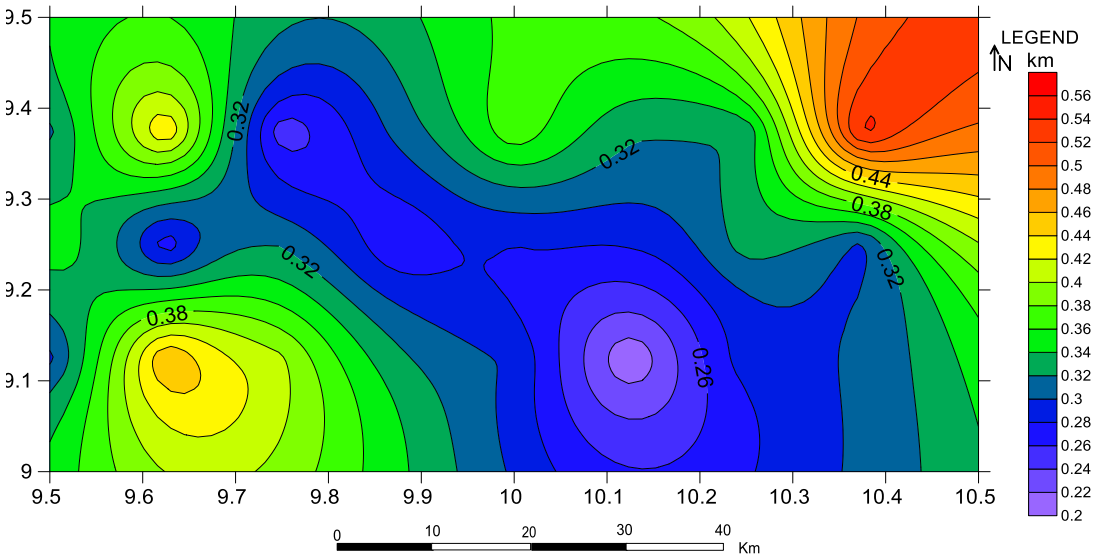


**Fig. 8: Spectral plots for all $D_2$ showing maximum depth of 0.58 km of the study area**

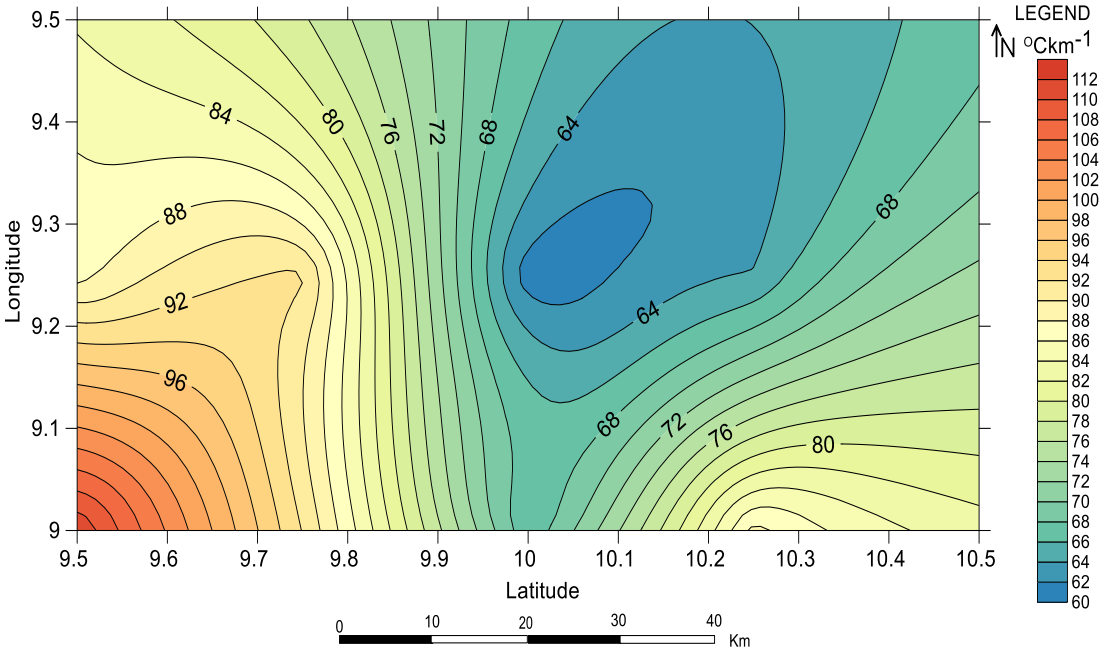


**Fig. 9: Geothermal gradient of the study area**

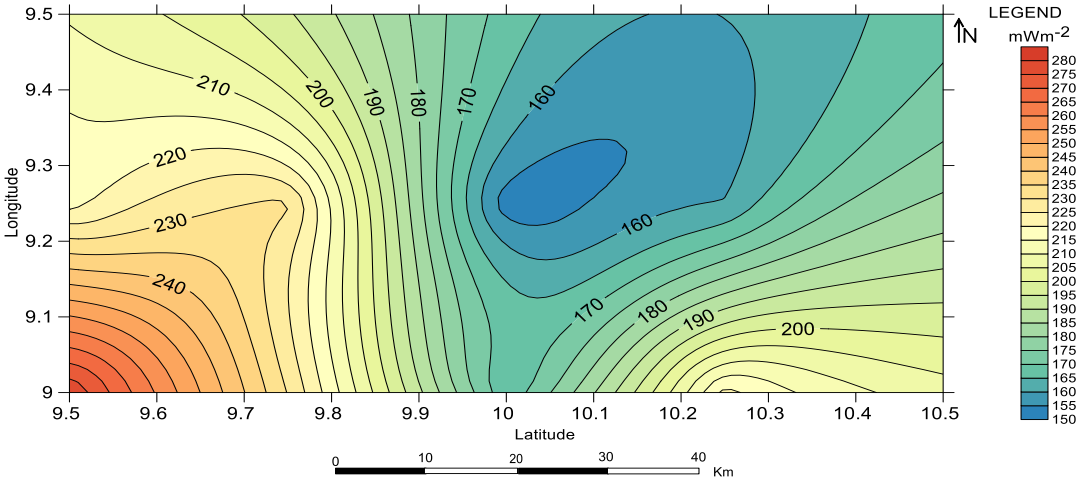


**Fig. 10: Heat flow of the study area**

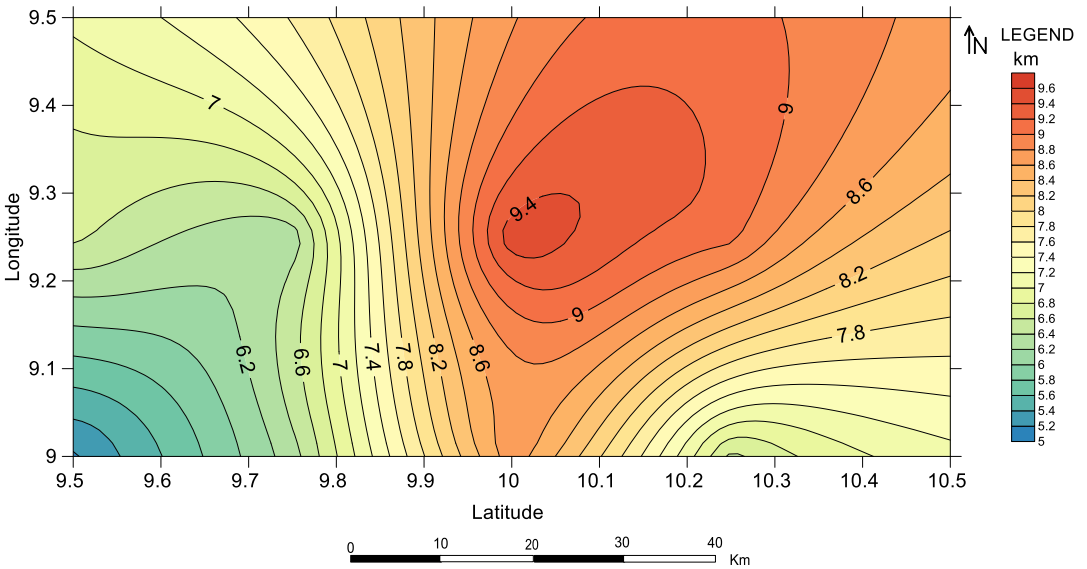


**Fig. 11: Curie point depth of the study area**

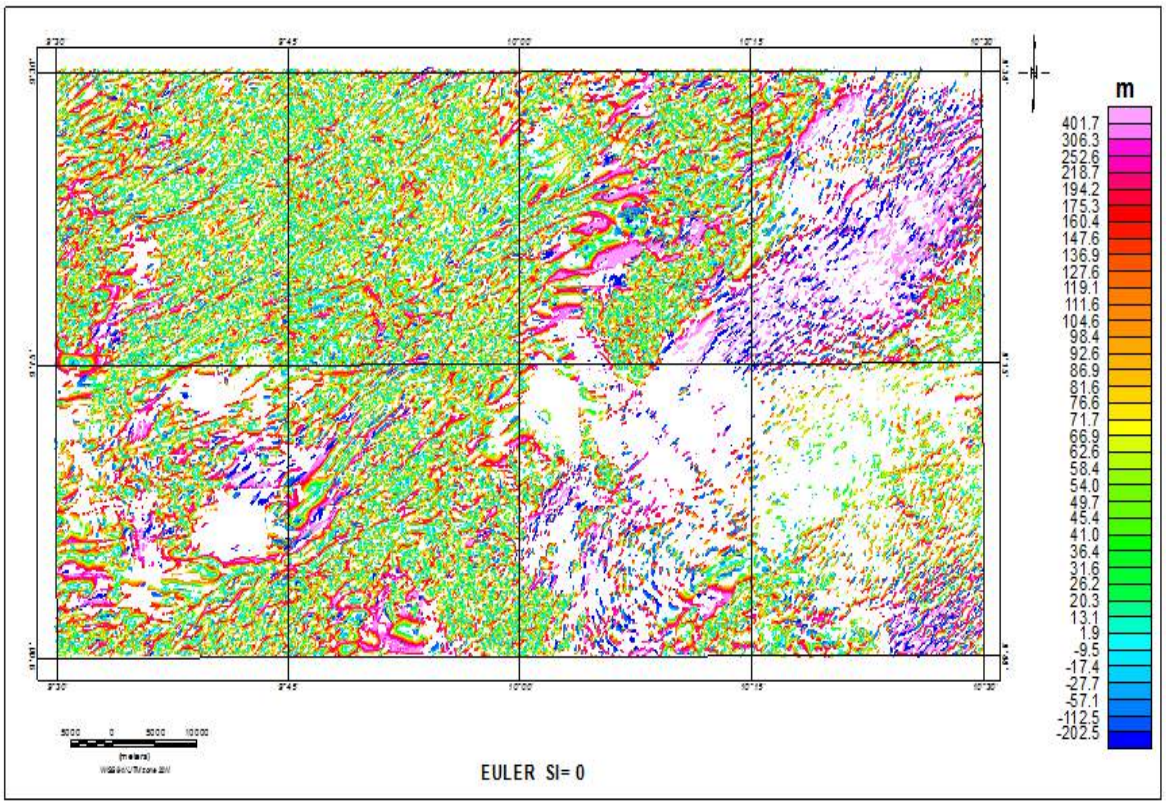


**Fig. 12: Euler Deconvolution map for SI=0**

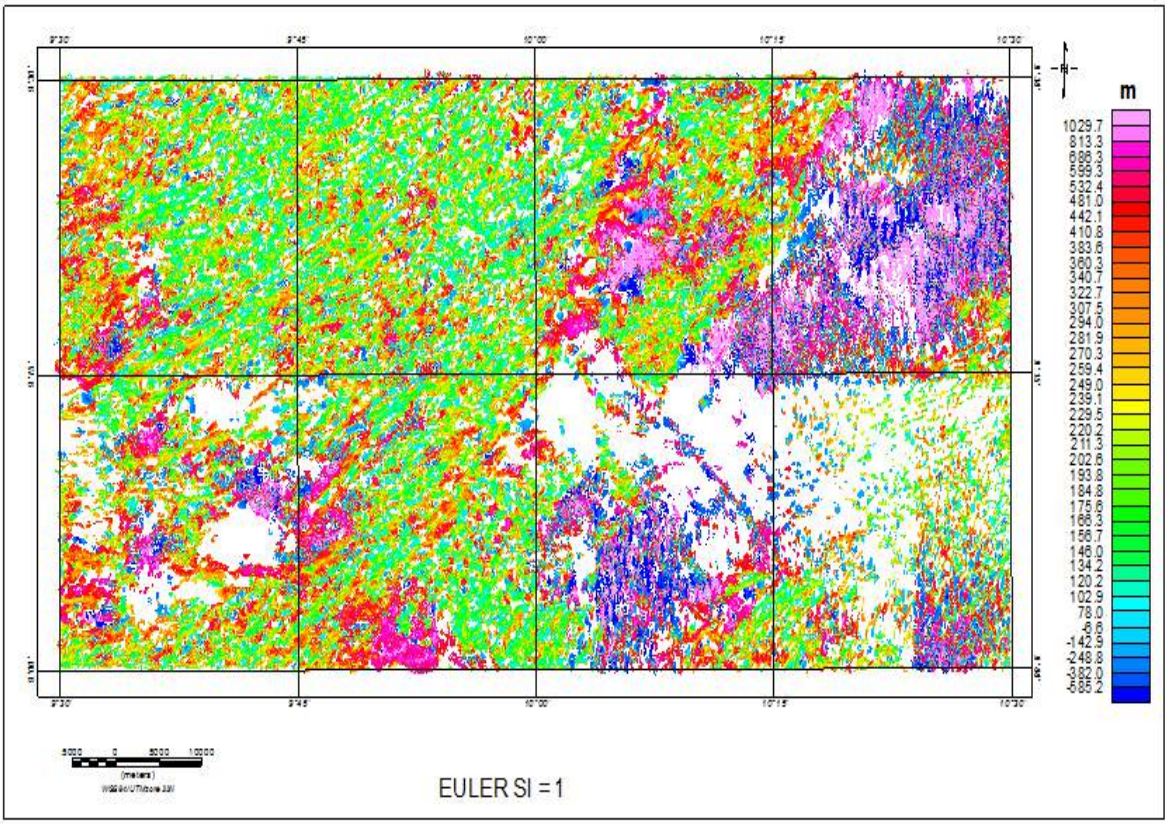


**Fig. 13: Euler Deconvolution map for SI=1**

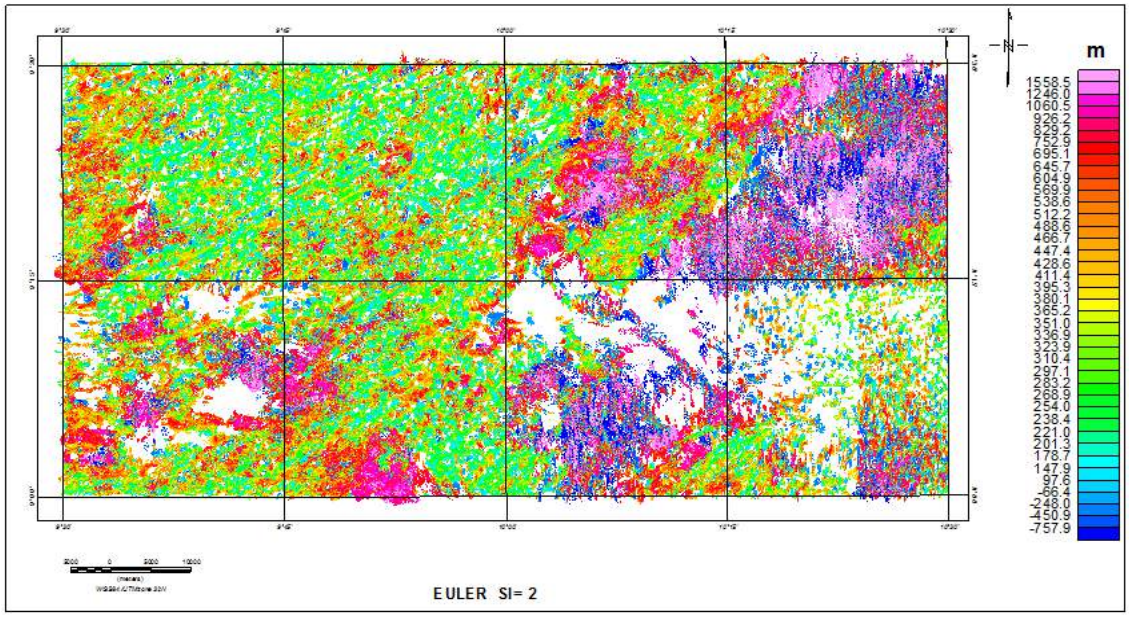


**Fig. 14: Euler Deconvolution map for SI=2**

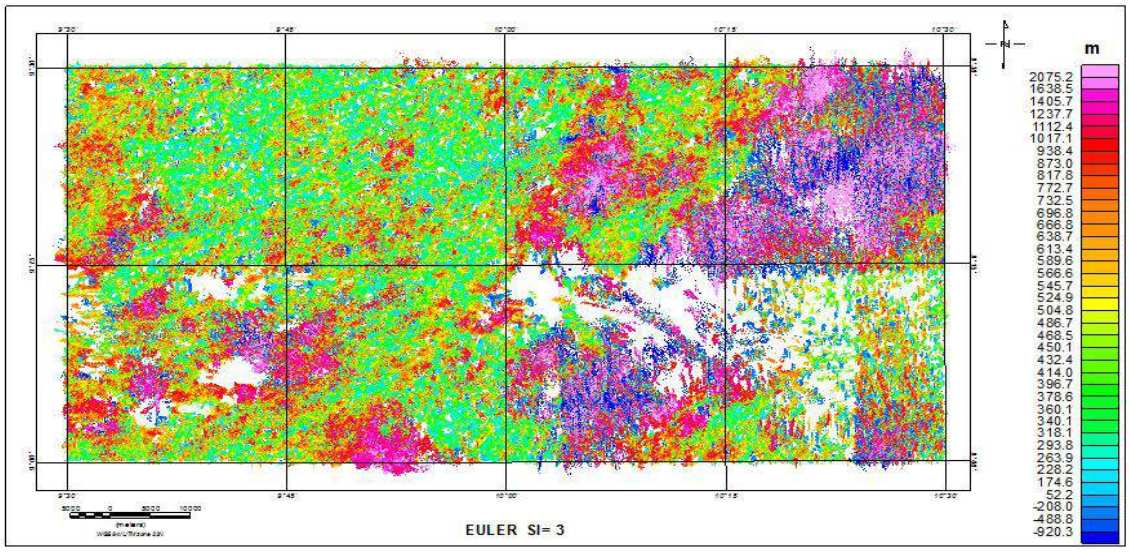


**Fig. 15: Euler Deconvolution map for SI=3**

To determine the depths of the anomalous magnetic sources, the RTE map of the study area was divided into 32 overlapping grids (Fig. 6). Each of these spectral blocks covers a square area of about 13.85 x 13.85 km of the data sheets and revealed two depths with depth to the first layer ($D_1$) which varies from 0.283 km to 3.04 km with an average depth of 1.367 km (Fig. 7). While the Second layer depth ($D_2$) which represent the shallow depth varies from 0.202 km to 0.547 km (Fig. 8) with the average depth of 0.327 km. The shallow depth ($D_2$) could be attributed to near surface magnetic sources, which are magnetic rocks that intruded into the sedimentary formations as a result of near surface intrusive and can be closely related to the tectonic and structural evolution of the study area.

The value of depth of first layer (0.283 - 3.04 km) is similar to the report of Bashar *et al*. (2017) where the depth- to-basement map suggested sedimentary thickness of 0.77 km to 2.31 km around Birnin Kebbi area. The deeper layer of magnetization from study area (0.283 km - 3.04 km) is lower than the deeper layer of magnetization from Yola area, Upper Benue Trough with depths ranging from 1.233 km to 4.013 km (Okereke *et al*., 2012).

The shallow depth in the present study is also similar to the work of Oghuma *et al*. (2015) where the shallow magnetic source ranges from 0.12 to 0.93 km, with an average depth of 0.572 km and was attributed to near surface magnetic sources, which are magnetic rocks that intruded into the sedimentary formations. Likkasson *et al*. (2005) equally worked around middle Benue Basin and obtained spectral matching yielding three dipoles equivalent source layers at 0.89 to 4.33 km and 18.22 km, where 4.33 km corresponds to maximum thickness within middle Benue Basin.

The D1 values obtained from the spectral plots therefore represent the average sedimentary thickness in the area. However, the depths obtained in this study agree with values obtained from other research works done by Ofoegbu (1984); Ofoegbu and Onuoha (1991) and Onwuemesi (1997). Wright *et al*. (1985) reported that when all other conditions for hydrocarbon accumulation are favourable, the minimum thickness of the sediment required for the commencement of oil formation would be 2.3 km. The basement depth of sedimentary thickness (0.283 - 3.04 km) in the present study is therefore capable of holding hydrocarbon potentials.

The depth from the present study is however lower than the depth obtained by Daniel *et al*. (2018) on modeling magnetic dykes with depth ranging from 1525.74 to 2919.21 km whereas the depth observed within the study area when cylindrical and spherical geological model was adopted ranges from -757.9 to 1558.5 m.

The geothermal gradient ranges from 60 to 112°C/km with an average value of 82.92°C/km (Fig. 9) and is higher than geothermal gradient of 30 to 44°C/km with an average value of 34°C/km reported by Nwankwo *et al*. (2011) from bottom hole temperature logs of Nupe Basin, Nigeria.

The heat flow ranges from 150 to 280 $mWm^{-2}$ (Fig. 10) which is higher than heat flow of 23.697 to 56.21°C/km reported by Udochukwu *et al*, (2019) from Monguno area, northeastern Nigeria. This is also higher than heat flow of 17.45 to 25.64ºC/km corresponding to mantle heat flow of about 46.00 to 67.60 mWm-2 reported by Anakwuba and Chinwuko (2015) from one dimensional spectral analysis of aeromagnetic data of eastern part of Chad Basin.

The Curie depth from spectral analysis ranges from 5.19 to 9.53 km (Fig. 11) with an average value of about 7.25 km (Table 2). The deepest (Red colour) Curie point depth lies at the northeastern part of Bashar while the shallowest (blue colour) Curie point depth was observed to be conspicuous in the Southwestern part of Wase. The Curie point depth value of the study area is lower than the Curie point depth value of 10.318 to 24.478 km reported by Udochukwu *et al.* (2019) from Monguno area, northeastern Nigeria

The region of high geothermal energy is characterized by an anomalous high temperature gradient and heat flow. It was therefore expected that geothermally active areas will be associated with shallow Curie point depth. From Table 2, the heat flow was inversely proportional to the Curie depth. Therefore, the heat flow in the study area increases with decreasing Curie isotherm depth (Fig. 11) while Figs. 9 and 10 give the direct nature of heat distribution in subsurface of the study area.

**Conclusion**

The depth to the first layer ($D_1$) which is the deeper depth varies from 0.283 to 3.04 km with an average depth of 1.367 km suggesting the occurrence of Precambrian Basement rocks. While the shallow depth $D_2$ varies from 0.202 to 0.547 km with the average depth of 0.327 km and could be attributed to near surface magnetic sources, which are magnetic rocks that intruded into the sedimentary formations. The heat flow increases with decrease in Curie point depth and the heat flow is significantly high suggestive of anomalous geothermal conditions. The average geothermal gradients and heat flow obtained is an indication that the area is suitable for harnessing of geothermal energy, which could be used to generate electricity.

**References**


Anakwuba EK & Chinwuko AI 2015. One-dimensional spectral analysis and currie depth isothermal of eastern Chad Basin, Nigeria. *Journal of Natural Sciences,* 19: 14-22.

Bashar MG, Sanusi YA & Udensi EE 2017. Interpretation of aeromagnetic data over Birnin-Kebbi and its adjoining areas using first vertical derivative and local wave number methods. *IOSR J. Appl. Geol. and Geophy.,* 5(5): 44-53.

Bhattacharyya BK & Leu LK 1975. Analysis of magnetic anomalies over Yellowstone National Park. Mapping the curie-point isotherm surface for geothermal reconnaissance. *J. Geophys. Res.,* 80: 461–465.

Carter JD, Barber W, Tait EA & Jones GP 1963. The geology of parts of Adamawa, Bauchi and Borno provinces in North-eastern Nigeria. Bull. *Geol. Surv. Nig.,* 30: 109-109.

Jacobson RRE, Snelling NJ & Truswell JF 1963. Age determination in the geology of Nigeria with special references to the older and younger granites. *Overseas Geol. and Mineral Resou.,* 9: 168–182.

Kangkolo R & Ojo SB 1997. Short comings in the determination of regional fields by polynomial fitting: A simple solution. *J. Appl. Geophy.,* 36: 205-212.

Likkasson OK, Ajayi CO & Shemang EM 2005. Some structural features of the middle Benue Trough, Nigeria, modeled from aeromagnetic anomaly data. *Science Forum: J. Pure and Appl. Sci.,* 8: 100-125.

Nwankwo LI, Olasehinde PI & Akoshile CO 2011. Heat flow anomalies from the spectral analysis of Airborne magnetic data of Nupe Basin, Nigeria. *Asian J. Earth Sci.,* 1(1): 6-13.

Ofoegbu CO 1984. Aeromagnetic anomalies over the Lower and Middle Benue Trough Nigeria. *Nig. J. Mining and Geol.,* 21: 103-108.

Ofoegbu, C.O., and Onuoha K.M. (1991).Analysis of magnetic data over the Abakaliki, anticlinorium of lower Benue trough, *Nigeria. Marine and Petroleum Geology,* 8: 174-183.

Okereke CN, Onu NN, Ibe KK & Selemo AO 2012. Analysis Of landsat and aeromagnetic data for mapping of linear structures: A case study of Yola Area, Upper Benue Trough, Nigeria. *Int. J. Engr. Res. and Applic.,* 2(3):1968-1977.

Onuba LN, Anudu GK, Chaiaghanam OI & Anakwuba EK 2015. Evaluation of aeromagnetic anomalies over Okigwe area South-Eastern Nigeria. *J. Envtal. and Earth Sci.,* 3: 498-507.

Onwuesemi AG 1997. One-dimensional spectral analysis of aeromagnetic anomalies and Currie depth isotherm in Anambra Basin of Nigeria. *Journal of Geodynamics,* 23(2): 95-107.

Oyawoye MO 1964. The geology of the Nigerian basement complex. *J. Nig. Mining Geol. and Metallurgical Soc.,* 1(2): 87 – 103.

Reeves C 2005. Aeromagnetic Survey, Principles, Practice and Interpretation, pp. 56-100.

Reid AB, Alisop JM, Granser H, Millet AJ & Somerton IW 1990. Magnetic interpretation in 3-dimension using Euler deconvolution. *Geophysics,* 55: 80-91.

Spector A & Grant FS 1970. Statistical models for interpreting aeromagnetic data. *Geophysics,* 35: 293-302.

Tanaka, A., Y., Okubo, & O. Matsubayashi, (1999), Curie point depth based on spectrum analysis of the magnetic anomaly data in East and Southeast Asia. *Tectonophysics,* 306: 3–4, 461–470.

Thompson DT 1982. A new technique for making computer-assisted depth estimates from magnetic data. *Geophysics,* 47: 31-37.

Udochukwu BC, Akiishi M & Tyovenda AA 2019. Estimation of geothermal gradient and heat flow for determination of geothermal energy resources in Monguno area of northeastern Nigeria. *J. Geogr., Envtal. and Earth Sci. Int.,* 20(1): 1-8.

Wright JB, Hastlings D, Jones WB & Williams HR 1985. Geology and Mineral Resources of West Africa. *Gorge Allen and Urwin London.*